A least-square high-order boundary element method for modelling ship waves

Hui Liang[a], **Jing Liu**[a], **Bhushan Taskar**[a]
a. Technology Centre for Offshore and Marine, Singapore (TCOMS), 118411, Singapore
Email: liang_hui@tcoms.sg

Highlights

- The study is based on the boundary integral equation free of waterline integrals;
- A least-square based high-order boundary element method is developed;
- The vector Green function for ship waves is derived and simplified.

1 Boundary-value problem

Consider a ship steadily translating in calm water of infinite depth along a straight path at a consistent speed U. A Cartesian coordinate system $Oxyz$ moving with the ship is defined with the Oxy plane coinciding with the undisturbed free surface and Oz axis pointing positively upward. Then, the velocity potential Φ in the flow field is

$$\Phi(x, y, z) = U[-x + \phi(x, y, z)], \tag{1}$$

where ϕ denotes the potential perturbed by the ship hull satisfying the Laplace equation $\nabla^2\phi = 0$. The velocity potential ϕ is determined by the boundary conditions. On the undisturbed free surface $z = 0$, it satisfies the linear Kelvin-Michell free surface condition

$$\frac{\partial^2\phi}{\partial x^2} + \kappa\frac{\partial\phi}{\partial z} = 0 \quad \text{at} \quad z = 0 \quad \text{with} \quad \kappa = \frac{g}{U^2}, \tag{2}$$

and the body boundary condition on the hull surface Σ^H given by

$$\frac{\partial\phi}{\partial n} = n_x \quad \text{on} \quad \Sigma^H, \tag{3}$$

where the normal vector $\mathbf{n} = (n_x, n_y, n_z)$ is defined positive pointing inwards the domain. By integrating the pressure over the body, the hydrodynamic force on the body is

$$\mathbf{F} = \iint_{\Sigma^H} p\,\mathbf{n}\,\mathrm{d}S \quad \text{with} \quad p = \rho U^2\left(\frac{\partial\phi}{\partial x} - \frac{1}{2}|\nabla\phi|^2\right). \tag{4}$$

2 Boundary integral equations

The boundary-value problem will be solved via establishing a boundary integral equation. By applying the Stokes theorem and free surface condition (2), the free surface integral is converted to a waterline integral, and we can obtain the boundary integral equation with a waterline integral, which is referred to as the "Neumann-Kelvin" model

$$\begin{aligned} 2\pi\phi(\mathbf{x}) = &\iint_{\Sigma^H}\left[n_\xi G(\mathbf{x};\boldsymbol{\xi}) - \phi(\boldsymbol{\xi})\frac{\partial G(\mathbf{x};\boldsymbol{\xi})}{\partial n(\boldsymbol{\xi})}\right]\mathrm{d}S \\ &- \frac{1}{\kappa}\oint_\Gamma\left[\frac{\partial\phi(\boldsymbol{\xi})}{\partial\xi}G(\mathbf{x};\boldsymbol{\xi}) - \phi(\boldsymbol{\xi})\frac{\partial G(\mathbf{x};\boldsymbol{\xi})}{\partial\xi}\right]\frac{n_\xi\mathrm{d}\ell}{\sqrt{n_\xi^2 + n_\eta^2}}, \end{aligned} \tag{5}$$

where $\mathbf{x} \equiv (x, y, z)$ and $\boldsymbol{\xi} \equiv (\xi, \eta, \zeta)$ denote the flow-field and singularity points, respectively, Σ^H is the mean wetted ship hull surface, Γ is the waterline of the ship hull, and $G(\mathbf{x}; \boldsymbol{\xi})$ is the ship-waves Green function which will be considered in § 3.

However, it has been demonstrated that the Neumann-Kelvin model is ill-posed. Moreover, the presence of the waterline integral brings considerable difficulties in the numerical implementation. To deal with these notorious issues, Noblesse et al. (2013) accounted for the component between the mean free surface and the actual free surface

$$\iint_{\Sigma_a^H} n_\xi G(\mathbf{x}; \boldsymbol{\xi}) \mathrm{d}S \approx \iint_{\Sigma^H} n_\xi G(\mathbf{x}; \boldsymbol{\xi}) \mathrm{d}S + \frac{1}{\kappa} \oint_\Gamma \frac{\partial \phi(\boldsymbol{\xi})}{\partial \xi} G(\mathbf{x}; \boldsymbol{\xi}) \frac{n_\xi \mathrm{d}\ell}{\sqrt{n_\xi^2 + n_\eta^2}}, \tag{6}$$

and introduced a vector Green function

$$\mathbf{G}(\mathbf{x}; \boldsymbol{\xi}) = (0, G_\zeta^\xi, -G_\eta^\xi) \quad \text{satisfying} \quad \nabla_{\boldsymbol{\xi}} G(\mathbf{x}; \boldsymbol{\xi}) = \nabla_{\boldsymbol{\xi}} \times \mathbf{G}(\mathbf{x}; \boldsymbol{\xi}) + (\partial^\xi \nabla_{\boldsymbol{\xi}}^2 G, 0, 0), \tag{7}$$

where subscript denotes differentiation, and superscript means integration. Then, a boundary integral equation free of waterline integral is obtained (He et al. 2021)

$$4\pi\phi(\mathbf{x}) = \iint_{\Sigma^H} \{ n_\xi G(\mathbf{x}; \boldsymbol{\xi}) + [\mathbf{n} \times \nabla_{\boldsymbol{\xi}} \phi(\boldsymbol{\xi})] \cdot \mathbf{G}(\mathbf{x}; \boldsymbol{\xi}) \} \, \mathrm{d}S, \tag{8}$$

which is referred to as the "Neumann-Michell model" (Noblesse et al. 2013). This paper is then devoted to numerically solving the Neumann-Michell model in Eq. (8).

3 Vector ship-wave Green function

The boundary integral equation (8) involves the vector Green function defined by (7). According to Liang & Chen (2019), the physically-realistic Green function for ship waves free of unbounded wave amplitude and extremely steep waves is expressed as

$$G(\mathbf{x}; \boldsymbol{\xi}) = -1/r + 1/r' + G^F(\mathbf{x}; \boldsymbol{\xi}), \text{ with } \{r, r'\} = \sqrt{(x-\xi)^2 + (y-\eta)^2 + (z \pm \zeta)^2}, \tag{9}$$

where G^F is a harmonic function responsible for free surface disturbance written as

$$G^F = \frac{2}{\pi} \mathrm{Re} \int_{-\infty}^{\infty} \int_0^{\infty} \frac{\mathrm{e}^{k(z+\zeta) - \mathrm{i}[\alpha(x-\xi) + \beta(y-\eta)]}}{U^2\alpha^2 - gk - 4\mathrm{i}U\nu\alpha k^2} \mathrm{d}\alpha \mathrm{d}\beta, \quad \text{with} \quad k = \sqrt{\alpha^2 + \beta^2}. \tag{10}$$

For free space Rankine source functions $1/r$ and $1/r'$, the components associated with the vector Green function given by Eq. (7) are written as

$$\begin{bmatrix} (1/r)_\zeta^\xi \\ (1/r)_\eta^\xi \end{bmatrix} = \frac{\mathrm{sign}(\xi - x)}{r(r + |\xi - x|)} \begin{bmatrix} \zeta - z \\ \eta - y \end{bmatrix}, \quad \text{and} \quad \begin{bmatrix} (1/r')_\zeta^\xi \\ (1/r')_\eta^\xi \end{bmatrix} = \frac{\mathrm{sign}(\xi - x)}{r(r + |\xi - x|)} \begin{bmatrix} \zeta + z \\ \eta - y \end{bmatrix}. \tag{11}$$

For the components associated with the free surface term G^F, they can be decomposed into local-flow and wave components $G^F = G^L + G^W$. Here we define nondimensional coordinates $(X, Y, Z) = \kappa(x - \xi, y - \eta, z + \zeta)$. Then, the local-flow components are written as

$$\begin{bmatrix} G^L \\ \partial_\zeta^\xi G^L \\ \partial_\eta^\xi G^L \end{bmatrix} = \frac{2\kappa}{\pi} \int_{-\pi/2}^{\pi/2} \begin{bmatrix} -\mathrm{sgn}(X) \, \mathrm{Im}[\mathrm{e}^{\mathbb{Z}} E_1(\mathbb{Z})] \, \cos\theta \\ \mathrm{sgn}(X) \, \mathrm{Re}[\mathrm{e}^{\mathbb{Z}} E_1(\mathbb{Z})] \, \cos^2\theta \\ -\mathrm{Re}[\mathrm{e}^{\mathbb{Z}} E_1(\mathbb{Z})] \, \sin\theta \cos\theta \end{bmatrix} \mathrm{d}\theta \tag{12}$$

where $\mathbb{Z} = [Z\cos\theta + \mathrm{sgn}(X)\, Y \, \sin\theta - \mathrm{i}X]$. The wave components are written as

$$\begin{bmatrix} G^W \\ \partial_\zeta^\xi G^W \\ \partial_\eta^\xi G^W \end{bmatrix} = 4H(-X)\mathrm{Im} \int_{-\infty}^{\infty} \begin{bmatrix} -\kappa \\ \mathrm{i}\kappa Q \\ -\kappa q \end{bmatrix} \exp\left[Q^2 Z + \frac{4\epsilon X Q^6}{Q^2 + q^2} - \mathrm{i}Q(X + qY) \right] \mathrm{d}q, \tag{13}$$

with $Q = \sqrt{1 + q^2}$.

4 Least-square high-order boundary element method

The inclusion of spatial derivatives within the boundary integral equation (8) necessitates the utilisation of high-order patches. In the conventional high-order boundary element method (HOBEM), the boundary integral equation is typically enforced at the nodal points of the patch, resulting in a determined equation system wherein the number of unknowns equals to the nodal points. However, challenges arise when the normal vector exhibits discontinuities at the edges or corners of a ship hull. Moreover, the study on removal of irregular frequencies (Liang et al. 2020) indicates that the equation system is not necessarily determined. Consequently, an overdetermined system can be efficiently solved using a least-square approach.

We aim to develop a least-square-based HOBEM by rendering the collocation points located within the patch as shown in Fig. 1. In this study, the six-node triangular quadratic patches are adopted, and then the velocity potential is interpolated as

$$\phi = \sum_{j=1}^{6} \phi_j \mathcal{N}_j(u, v), \quad \text{with} \quad 0 \leq u + v \leq 1, \tag{14}$$

where u and v are parametric coordinates, and $\mathcal{N}_j(u, v)$ are shape functions. The spatial derivatives of the velocity potential can be obtained by differentiating shape functions.

The boundary integral equation is enforced on collocation points situated within each patch, unlike the traditional HOBEM where collocation points coincide with the nodes. In this method, three such points are allocated per patch at $(u_1, v_1) = (2/15, 2/15)$, $(u_2, v_2) = (11/15, 2/15)$, and $(u_3, v_3) = (2/15, 11/15)$ in the parametric coordinate system, as illustrated in Fig. 1. Typically, the number of nodes within the quadratic boundary element method ranges from 2 to 3 times the number of patches. This results in an overdetermined equation system with more equations than unknowns. While computing influence coefficients, there are three specific scenarios. (1) When the collocation point is distant from the influence patch, direct allocation of Gaussian points is executed. (2) If the collocation point lies near the patch but outside it, the patch is subdivided into four subpatches. (3) When the collocation point locates within the patch, the patch is splitted into three subpatches as in Fig. 1. The influence of each subpatch on the collocation point is realised by the transformation of triangle polar coordinates.

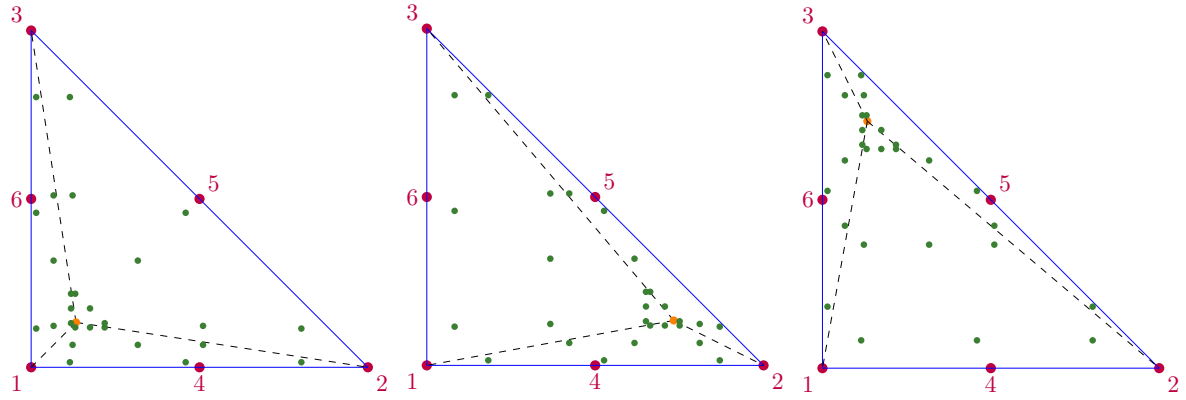

Figure 1: Allocation of Gaussian points (●) on a triangular patch composed of six nodes (●) when the collocation point (●) located within the patch.

5 Preliminary results

As an illustrative numerical example, we investigate the wave drag exerted on a submerged ellipsoid moving steadily beneath a free surface. The ellipsoid has major and minor axes of $2a = 2.3$ m and $2b = 0.4$ m respectively, resulting in a focal distance of $c = \sqrt{a^2 - b^2} = 1.132$ m. The submergence ratio of the ellipsoid is $d/c = 0.252$. In Fig. 2, we present the nondimensional wave drag, denoted as $f_x = -1000F_x/(\pi\rho g c^3)$, varying with the Froude number $F = U/\sqrt{2gc}$. Comparison is made with the numerical solution by Chen et al. (2001). The generally good agreement validates the reliability of our numerical method. Additional results will be presented at the workshop, including further analyses on the wave drag and wave patterns generated by a surface-piecing ship hull.

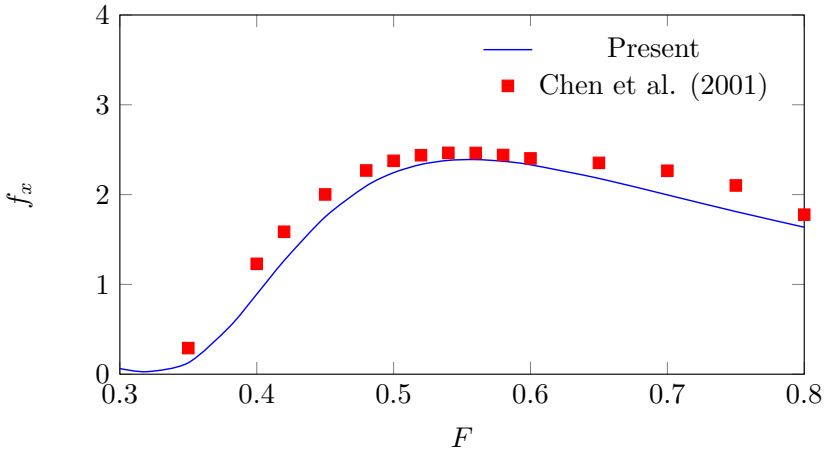

Figure 2: Wave drag experienced by a submerged ellipsoid beneath a free surface varying with the Froude number.

Acknowledgement: This work is supported by the National Research Foundation, Singapore and Singapore Maritime Institute under the Maritime Transformation Programme White Space Fund (Centre of Excellence for Autonomous and Remotely Operated Vessels (CEAOPS), Project ID SMI-2019-MTP-01).

References

Chen, X. B., Diebold, L. & Doutreleau, Y. (2001), New Green-function method to predict wave-induced ship motions and loads, *in* 'Proceeding of the 23rd Symposium on Naval Hydrodynamics, Val de Reuil, France', pp. 66–81.

He, J., Wu, H., Yang, C.-J., Zhu, R.-C., Li, W. & Noblesse, F. (2021), 'Boundary-integral representation sans waterline integral for flows around ships steadily advancing in calm water', *European Journal of Mechanics-B/Fluids* **89**.

Liang, H. & Chen, X. B. (2019), 'Viscous effects on the fundamental solution to ship waves', *Journal of Fluid Mechanics* **879**, 744–774.

Liang, H., Ouled Housseine, C., Chen, X. B. & Shao, Y. (2020), 'Efficient methods free of irregular frequencies in wave and solid/porous structure interactions', *Journal of Fluids and Structures* **98**, 103130.

Noblesse, F., Huang, F. & Yang, C. (2013), 'The Neumann–Michell theory of ship waves', *Journal of Engineering Mathematics* **79**(1), 51–71.